European Journal of Remote Sensing

ISSN: 2279-7254 (Online) Journal homepage: www.tandfonline.com/journals/tejr20

Spatio-temporal assessment of *Toumeyella parvicornis* spread in mediterranean coastal pine forests through sentinel-2 data

Giovanni D'Amico

To cite this article: Giovanni D'Amico (2026) Spatio-temporal assessment of *Toumeyella parvicornis* spread in mediterranean coastal pine forests through sentinel-2 data, European Journal of Remote Sensing, 59:1, 2709014, DOI: 10.1080/22797254.2026.2709014

To link to this article: https://doi.org/10.1080/22797254.2026.2709014

EUROPEAN JOURNAL OF REMOTE SENSING
2026, VOL. 59, NO. 1, 2709014
https://doi.org/10.1080/22797254.2026.2709014

Taylor & Francis
by informa

RESEARCH ARTICLE

OPEN ACCESS Check for updates

Spatio-temporal assessment of *Toumeyella parvicornis* spread in mediterranean coastal pine forests through sentinel-2 data

Giovanni D'Amico

geoLAB - Laboratory of Forest Geomatics, Department of Agriculture, Food, Environment and Forestry (DAGRI), University of Florence, Firenze, Italy

ABSTRACT

Mediterranean coastal pine forests offer vital ecological and cultural benefits but face threats from climate change, urbanization, and pests. Among invasive agents, *Toumeyella parvicornis* is a severe threat to *Pinus pinea* along Italy's coast, causing canopy loss and death. Despite many studies on outbreak detection, the regional-scale dynamics and risk factors are poorly understood. Thus, an interpretable remote sensing framework using multitemporal Sentinel-2 composites to track *T. parvicornis* infestation in Campania, Italy, from 2017 to 2025 was developed. Seasonal medoid composites and spectral indices were generated in Google Earth Engine. Random Forests and SHAP interpretation assessed infestation patterns, vulnerability, and risk. The workflow combined spectral, temporal, and spatial predictors, including interannual differences, proximity to previous infestations, and transportation infrastructure. Annual attack-transition, vulnerability, and risk maps were produced and validated with photointerpretation data. The attack-transition model had an AUC of 0.79, whereas the vulnerability model showed only moderate discrimination and should be interpreted as a high-sensitivity screening layer rather than as a binary prediction product. The risk model achieved an AUC of 0.80, providing more robust operational prediction of near-future infestation. This scalable framework aids in monitoring invasive pests and understanding environmental conditions and exposure-related spatial factors associated with *T. parvicornis* spread.

ARTICLE HISTORY
Received 10 June 2026
Revised 10 July 2026
Accepted 13 July 2026

KEYWORDS
Canopy stress; explainable artificial intelligence; forest disturbance; forest risk; forest vulnerability; invasive pests; spatio-temporal modelling

Introduction

Mediterranean coastal pine forests are highly valuable ecosystems that provide multiple ecological, protective, and socio-cultural functions. In addition to their role in dune stabilisation and coastal protection, these forests contribute to biodiversity conservation, carbon sequestration, recreational activities, and landscape identity across Mediterranean regions. In Italy, coastal pine forests dominated by *Pinus pinea* are among the most characteristic elements of coastal landscapes and are frequently embedded within urban, peri-urban, and protected coastal systems (Bonari et al., 2017, 2021; Nicoletti et al., 2024).

In recent decades, Mediterranean forests have been increasingly exposed to interacting stressors, including climate warming, prolonged droughts, land-use changes, urban expansion, and biological disturbances. These processes have intensified forest decline and increased tree susceptibility to insect outbreaks and pathogens (Seidl et al., 2017; Senf & Seidl, 2021; Sommerfeld et al., 2018). Insect outbreaks are becoming more frequent and severe in Mediterranean forests, where warming can affect insect survival, development, and range expansion, while drought can reduce tree vigour and resistance (Hlásny et al., 2021; Park Williams et al., 2013). Coastal pine ecosystems are particularly vulnerable due to their fragmented distribution, anthropogenic pressures, and recurrent exposure to heat and water stress.

Among recent invasive agents affecting Mediterranean pine forests, *Toumeyella parvicornis* (pine tortoise scale) has become one of the most critical emerging threats. Native to North America, *T.*

CONTACT Giovanni D'Amico giovanni.damico@unifi.it geoLAB - Laboratory of Forest Geomatics, Department of Agriculture, Food, Environment and Forestry (DAGRI), University of Florence, Via San Bonaventura 13, Firenze, 50145, Italy
Supplemental data for this article can be accessed online at https://doi.org/10.1080/22797254.2026.2709014.

parvicornis was first recorded in Campania in 2014, where the pest rapidly affected urban and coastal pine stands (Garonna et al., 2015, 2018). Subsequent official and scientific records documented its occurrence in Rome, and in other Italian regions, including Abruzzo and Apulia (Bascietto et al., 2025; Bragard et al., 2022; Falanga et al., 2024; Tagarelli et al., 2022). Outside Italy, the species was officially reported in southern France in 2021, and subsequently in Albania, where a first record was confirmed by morphological and molecular analyses (Di Sora et al., 2024; EPPO, 2026). The insect feeds on pine sap, producing abundant honeydew and promoting the development of sooty moulds, progressively reducing photosynthetic activity, canopy vigour, and tree vitality. Severe infestations may lead to defoliation, canopy collapse and tree mortality (Bascietto et al., 2025; Garonna et al., 2018; Niccoli et al., 2024).

The growing availability of remote sensing data has considerably improved the ability to monitor forest disturbances across large spatial and temporal scales. Optical remote sensing has been widely used to detect insect-related disturbances because vegetation stress modifies canopy reflectance, phenology, and spectral trajectories before, during, and after outbreak development (Huo et al., 2024; Senf et al., 2017; Stone & Mohammed, 2017). Sentinel-2 is particularly suitable for forest health monitoring because its visible, near-infra-red, short-wave infra-red, and red-edge bands allow the characterisation of canopy structure, chlorophyll content, and moisture conditions at high temporal frequency and medium spatial resolution (Bárta et al., 2021; Dalponte et al., 2022; Drusch et al., 2012; Lastovicka et al., 2020). Similar approaches have been successfully applied to bark beetle outbreaks and other forest pest disturbances, including Landsat-based infestation dynamics, Sentinel-2 multi-temporal monitoring frameworks, and machine learning approaches for mapping affected conifer stands (Andresini et al., 2023; Bozzini et al., 2023; Candotti et al., 2022; Goodwin et al., 2008).

Several recent studies have investigated remote sensing approaches for detecting *T. parvicornis* impacts on Mediterranean pine forests. In Campania, Sentinel-2 vegetation indices were used to analyse spectral degradation in the Domitian coastal pine forest over the 2016–2022 period (Nicoletti et al., 2024), while dendrochronological, isotopic, and satellite analyses showed that enhanced vegetation index (EVI) and normalised difference moisture index (NDMI) were particularly informative for detecting canopy decline and moisture-related dynamics in a severely affected *Pinus pinea* stand (Niccoli et al., 2024). In Rome, PlanetScope time series enabled near-real-time detection of damaged trees through vegetation index thresholds (Falanga et al., 2024), while multi-platform analyses at Castelporziano combined very high resolution imagery, Sentinel-2, and PlanetScope to monitor insect outbreak progression and evaluate near-real-time detection performance (Petti et al., 2026). A further study integrated Sentinel-2 and PRISMA hyperspectral imagery to detect symptomatic stands and test dispersal hypotheses, finding limited evidence for prevailing wind as the main driver and suggesting the possible role of roads, traffic corridors, wind tunnels and local landscape conditions (Bascietto et al., 2025).

Despite these advances, existing studies still provide limited evidence on how infestation spreads at regional scales and on which spectral and spatial conditions make pine stands more likely to be affected. Most existing studies focus on outbreak detection, temporal degradation signals, threshold-based discrimination, or local-scale monitoring. On the other hand, integrating multitemporal Sentinel-2 indicators, interannual spectral changes, and spatial exposure variables into interpretable machine learning frameworks that can distinguish infestation occurrence, vulnerability, and risk remains understudied.

In this study, infestation transition refers to the probability that a pine stand shifts from a pre-attack condition to the onset of detectable infestation in a given year. Vulnerability is interpreted as the predisposition of coastal pine forests to experience infestation-related canopy decline when exposed to *T. parvicornis*, whereas risk is interpreted as the spatial probability of infestation occurrence or intensification resulting from the interaction between vulnerability and exposure to infestation sources and potential dispersal pathways. This terminology follows the broader risk framework in which risk depends on the interaction between hazard, exposure, and vulnerability, while adapting it to a spatial forest-health context (Forzieri et al., 2020; IPCC, 2012).

In this context, the present study aimed to reconstruct the spatio-temporal evolution of *T. parvicornis* infestation across coastal pine forests in Campania between 2017 and 2025 using multitemporal Sentinel-2 summer composites and Random Forest modelling. Specifically, the study aimed to: (i) map annual attack-transition dynamics; (ii) identify the most informative spectral and temporal predictors associated with

canopy decline; (iii) model near-future forest vulnerability; and (iv) estimate spatial risk by integrating vulnerability with infestation pressure and exposure to transportation and coastal gradients.

To support interpretation without imposing an a priori ecological ranking of predictors, candidate variables were retained in the Random Forest model after redundancy filtering, and their contributions were assessed a posteriori using model-based importance measures and SHAP values.

Random Forest was used to account for nonlinear relationships among spectral, temporal, and spatial variables (Breiman, 2001). SHAP, or SHapley Additive exPlanations, is an explainable artificial intelligence approach that decomposes each model prediction into additive feature contributions, allowing both the magnitude and direction of predictor effects to be evaluated (Lundberg & Lee, 2017; Molnar, 2022). Because Sentinel-2 bands, vegetation indices and interannual differences are partly correlated, results were interpreted at both individual-predictor and predictor-group levels to reduce overinterpretation of single correlated variables (Strobl et al., 2008).

Materials

Study area

The study was conducted across coastal pine forests located in the Campania region (Southern Italy), the earliest and most severely affected areas invaded by *Toumeyella parvicornis* in Europe. Specifically, the first European outbreak of the species was reported in Campania in 2014, where severe infestations rapidly affected *Pinus pinea* stands along the Tyrrhenian coast (Garonna et al., 2015, 2018).

The investigated forests are mainly distributed along the sea coastline and are dominated by *Pinus pinea*, frequently associated with *Pinus pinaster*, *Pinus halepensis,* and Mediterranean evergreen vegetation. Many of these coastal pine forests originated from twentieth-century reforestation and coastal management activities aimed at stabilising sandy dune systems, protecting inland areas, and shaping the coastal landscape (Nicoletti et al., 2024). Mediterranean pine forests are among the most characteristic ecological and landscape features of coastal and urban environments in central and southern Italy, where they provide significant ecological, recreational, and protective services (Nicoletti et al., 2024; Petti et al., 2026). These pine systems are widely distributed within urban and peri-urban areas, where increasing anthropogenic pressure, fragmentation, and climate-related stress contribute to forest vulnerability.

The study area is characterised by a Mediterranean climate with hot, dry summers and mild, wet winters. Pine forests mainly develop on coastal sandy dune systems exposed to intense urbanisation, transportation infrastructures, and touristic activities. Such conditions make these ecosystems particularly vulnerable to biological invasions and forest decline processes.

Overall, approximately 4,357 ha of coastal pine forests were included in the analysis. Since the first detection of *T. parvicornis*, the infestation progressively expanded along the regional coastal belt, causing severe decline and mortality in several pine stands. The Campania region, therefore, represents a particularly suitable case study for investigating the regional dynamics of *T. parvicornis* spread across Mediterranean coastal pine forests.

Reference data

Reference data were derived from official observations of *Toumeyella parvicornis* occurrences provided by the Campania Regional Plant Protection Service and made publicly available through the regional monitoring platform (Regione Campania, 2025). The original dataset consisted of georeferenced occurrence points documenting the presence of infestation across the region. To reconstruct infestation dynamics from 2017 to 2025, these observations were revised through multitemporal visual photointerpretation using regional orthophotos, Google Earth historical imagery, and PlanetScope imagery where available.

The revision aimed to improve the temporal consistency of the reference dataset and to ensure spatial coherence between reported occurrences, visible canopy symptoms, and infestation-related decline patterns. Photointerpretation was based on the visual identification of canopy discoloration, thinning, crown transparency, progressive decline, and, where evident, tree mortality patterns consistent with *T.*

parvicornis infestation. The assigned onset year corresponded to the first year in which infestation-related canopy decline was clearly detectable in the multitemporal image sequence. When symptoms appeared gradual or image availability did not allow an unambiguous attribution, the onset year was assigned conservatively to the first year of clear visual evidence. Under these conditions, a residual temporal uncertainty of approximately ± 1 year was considered plausible.

Following the revision, a final set of 200 reference samples was retained, covering infestation onset years from 2017 to 2025 (Figure 1). To assess the temporal consistency of the photointerpreted onset year, spectral trajectories of key Sentinel-2 summer predictors were extracted within the reference polygons for the years preceding and following the assigned onset. Mean polygon values of Sentinel-2 spectral indices (see section 2.3) were aligned relative to the onset year and inspected to verify whether the assigned year corresponded to the beginning of a persistent decline in canopy greenness, moisture status, or red-edge-related indicators. This analysis was used as an internal consistency check of the temporal attribution procedure rather than as an independent validation dataset (Figure S1).

The revised reference dataset was then used to generate model-specific sample-year tables. For the attack-transition model, positive samples corresponded to the assigned onset year, whereas negative samples were derived from years occurring at least three years before the assigned onset. The two years immediately preceding the onset and all post-disturbance years were excluded to reduce temporal uncertainty and to avoid training the classifier on intermediate or chronic degradation conditions. For vulnerability and risk modelling, observations at year t were linked to infestation occurrence in year $t + 1$. This formulation allowed the same reference observations to support different temporal modelling tasks while reducing leakage among pre-attack, attack, and post-disturbance conditions. The resulting reference and sample-year datasets are summarised in Table 1.

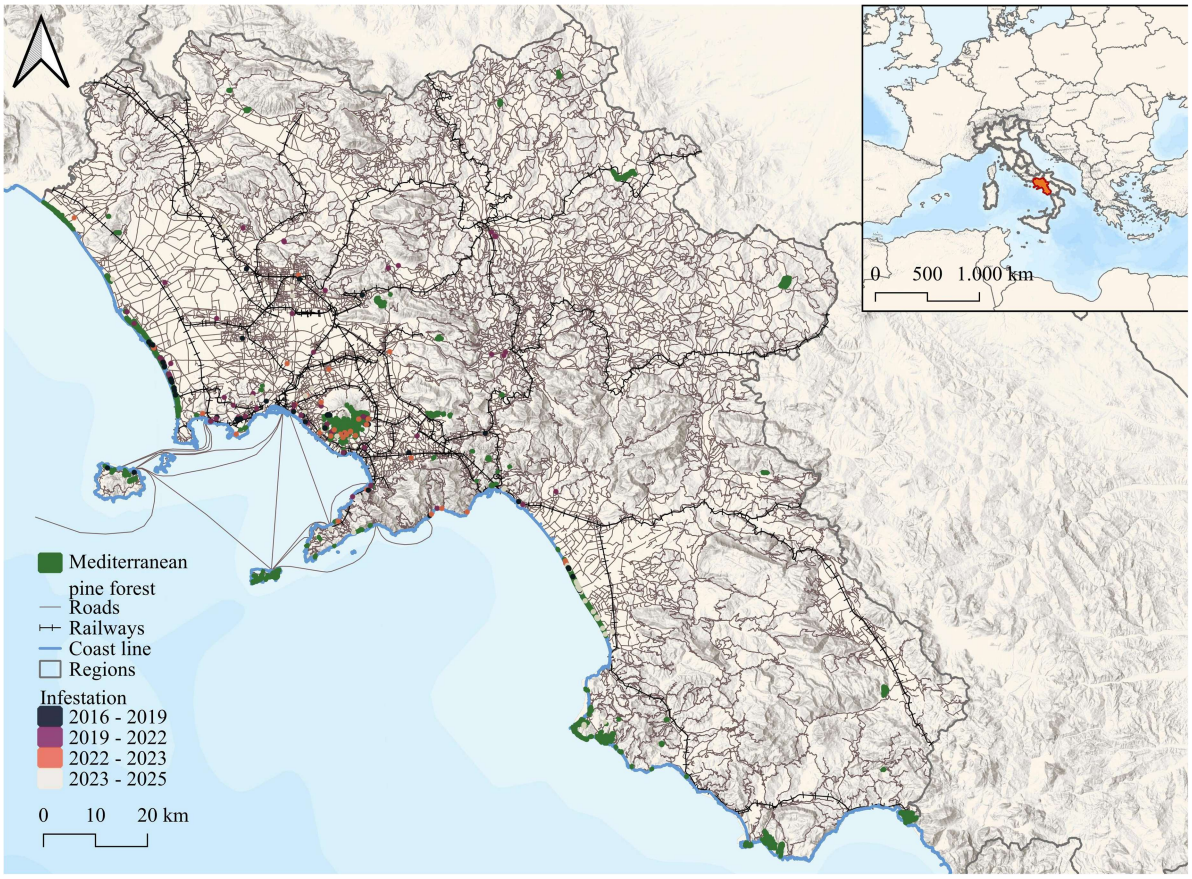

Figure 1. Area of interest defined as spatial distribution of Mediterranean pine forests within the study area across Campania, along with major transportation infrastructure and reference infestation-onset point, grouped by period.

Table 1. Reference data and sample-year datasets used for model calibration.

Dataset	Rows	Positive	Negative	Use
Reference points	200	—	—	Revised occurrence points with infestation-onset year assigned by photo-interpretation
Attack transition	422	130	292	Current-year infestation onset, with negative samples from years at least three years before onset
Vulnerability and Risk	987	119	868	Predictors at year *t* linked to infestation occurrence at year *t*+1

Sentinel-2 dataset and preprocessing

Sentinel-2 Level-2A Surface Reflectance Harmonised imagery available in Google Earth Engine was used to generate annual summer composites for the 2017–2025 period (Drusch et al., 2012; Gorelick et al., 2017). The analysis was restricted to summer because Mediterranean coastal pine forests experience pronounced seasonal water stress during the dry season, and canopy symptoms related to *T. parvicornis* are expected to be more spectrally detectable under these conditions. This choice is consistent with previous remote-sensing studies on Mediterranean pine decline and *T. parvicornis*, which showed that summer Sentinel-2 vegetation indices, moisture-sensitive indicators, and cloud-free composites are informative for detecting infestation-related canopy degradation (Bascietto et al., 2025; D'Amico et al., 2023; Nicoletti et al., 2024; Niccoli et al., 2024; Petti et al., 2026). For each year, images within a 30-day temporal window centred on 1 August were filtered using Sentinel-2 cloud probability and Scene Classification Layer information to remove clouds, cloud shadows, and other atmospheric contaminants. The 30-day window was selected to reduce phenological variability while preserving the summer signal and ensuring sufficient cloud-free observations. Seasonal medoid composites were then generated to preserve physically consistent spectral responses and reduce the influence of residual outliers (Flood, 2013). All products were generated at a 10 m spatial resolution and clipped to the coastal pine-forest mask.

The predictor combined Sentinel-2 spectral bands (Drusch et al., 2012), vegetation indices, and interannual change metrics (Table 2). Vegetation indices included normalised difference vegetation index (NDVI) (Rouse et al., 1973), normalised burn ratio (NBR) (Key & Benson, 2006), EVI (Huete et al., 2002), NDMI (Gao, 1996), normalised difference water index (NDWI) (McFeeters, 1996), normalised difference Red-Edge index (NDRE) (Delegido et al., 2011), chlorophyll Red-Edge (CI_RE) (Gitelson et al., 2003), and Red-Edge position index (REPO) (Gholizadeh et al., 2016). Absolute annual differences were computed as $X_t - X_{t-1}$, whereas normalised annual differences were computed as $(X_t - X_{t-1})/|X_{t-1}|$ (Candotti et al., 2022; Goodwin et al., 2008; Lastovicka et al., 2020; Senf et al., 2017). These temporal metrics were included to capture both the magnitude of canopy change and the relative intensity of spectral decline relative to the previous-year condition. Red-edge and moisture-sensitive predictors were retained because they are expected to respond to chlorophyll decline, canopy degradation, and water-related stress in coniferous stands affected by biotic disturbances (Bascietto et al., 2025; Niccoli et al., 2024).

Static spatial predictors were generated from roads, railways, and coastline layers, yielding Euclidean distance and normalised proximity measures that represented exposure to transport corridors and coastal gradients. In addition, annual infestation-pressure predictors were derived from the attack-transition maps (Bascietto et al., 2025). For each observation year, attack probabilities were binarized using the 0.50 threshold, and two pressure variables were derived within the pine-forest mask: distance to attack, defined as the Euclidean distance to the nearest predicted attacked pixel and capped at 5000 m, and attack density, defined as the proportion of predicted attacked pixels within a 7×7 pixel moving window, corresponding to a focal radius of three Sentinel-2 pixels. These variables were used only in the risk model to represent spatial exposure to previously detected infestation patterns and local neighbourhood pressure (Table 2).

Table 2. Predictor groups included in the modelling framework.

Predictor group	Predictors	Interpretation
Sentinel-2 bands	B2–B12	VIS, red-edge, NIR, SWIR response
Spectral indices	NDVI, NBR, EVI, NDMI, NDWI, NDRE, CI_RE, REPO	Vigour, moisture, chlorophyll
Absolute differences	$X_t - X_{t-1}$	Magnitude of change
Normalised differences	$(X_t - X_{t-1})/\|X_{t-1}\|$	Normalised magnitude of change
Static proximity	roads, railways, coast	Exposure gradients
Infestation pressure	dist_attack, dens_attack	Predicted attacked pixels gradients

Methods

Overview of the modelling framework

The modelling framework was structured to produce three sequential probability maps: attack transition, vulnerability, and risk. The attack-transition map reconstructed the annual onset of infestation across the monitored pine forests. The vulnerability map estimated near-future susceptibility from Sentinel-2 spectral and temporal predictors observed before the target year. The risk map then combined vulnerability with infestation pressure and spatial exposure predictors to represent areas where susceptible pine stands were also more exposed to previous attacks and to potential dispersal pathways.

The workflow included four main analytical steps: generation of annual summer Sentinel-2 predictors, Random Forest modelling of the three probability maps, interpretation of model outputs through model-based importance and SHAP values, and quantification of annual high-probability areas and their overlap with next-year attack. This structure enabled the assessment of infestation detection, pre-attack susceptibility, and spatially explicit risk within a single, temporally consistent framework.

Random forest model implementation

Random Forest is an ensemble learning method that builds multiple decision trees from bootstrap samples of the training data and combines their predictions through majority voting for classification tasks (Breiman, 2001). This approach is suitable for remote sensing applications because it can model nonlinear relationships, handle interactions among predictors, and is relatively robust to noisy and correlated input variables (Belgiu & Drăguţ, 2016). In this study, Random Forest was used to estimate class probabilities rather than only hard class labels, allowing the resulting maps to be interpreted as continuous probability maps.

Models were implemented in Python using the scikit-learn RandomForestClassifier and were trained separately for attack transition, vulnerability, and risk using the sample-year datasets described in Section 2.2. For each model, 500 trees were grown using the Gini impurity criterion. The number of features considered at each split was set to the square root of the total number of predictors, and the minimum number of samples required at each leaf node was set to 1. No maximum tree depth was imposed. Class weights were not applied. Model training was performed using a fixed random seed of 42 to ensure reproducibility. No formal hyperparameter tuning was applied; instead, the same core modelling configuration was used across the three components to preserve comparability among attack transition, vulnerability, and risk models.

The attack-transition and vulnerability models used automatic selection of the most informative predictors from the available Sentinel-2 candidate pool, after excluding highly correlated variables using a correlation threshold of 0.92. The risk model was instead fitted using a fixed set of six predictors: predicted vulnerability, distance from previous attacks, local attack density, and proximity to roads, railways, and coastline.

The final candidate sets included 17 predictors for attack transition, 22 for vulnerability, and 6 for risk. A formal wrapper-based feature selection procedure was not applied. Instead, candidate predictors were filtered to reduce redundancy among highly correlated variables and to retain a moderate number of ecologically interpretable predictors. All predictors retained in the candidate feature sets were used for model fitting, and their contributions were evaluated a posteriori using model-based importance measures and SHAP values.

Model evaluation and threshold definition

Model performance was assessed using grouped 10-fold cross-validation, with folds defined at the reference-point level to avoid placing observations from the same location in both calibration and validation subsets. Grouped cross-validation was adopted to reduce information leakage caused by repeated temporal observations associated with the same reference location. In this scheme, all sample-year records derived from the same reference point were assigned to the same fold, ensuring that observations from a given location were never used simultaneously for model calibration and validation.

Grouped cross-validation was selected because the main source of repeated non-independence in the sample-year dataset was the temporal reuse of the same reference locations. Assigning all records from the same reference point to the same fold prevented direct leakage between calibration and validation. A full spatial-block cross-validation was not implemented because the monitored pine forests are distributed along a narrow and discontinuous coastal belt, where spatial blocks would have produced highly unbalanced folds in terms of forest area, infestation years, and positive samples. Therefore, grouped cross-validation was considered the most appropriate compromise for evaluating model discrimination while preserving comparable class representation across folds.

To avoid information leakage between the vulnerability and risk modelling stages, the vulnerability probabilities used as predictors in the risk model were generated out of fold. For each grouped cross-validation fold, the vulnerability model was fitted only on the training groups and used to predict the held-out groups; the same group partition was then retained for risk-model calibration and validation. Therefore, observations in each validation fold did not contribute to estimating their vulnerability values or to risk-model calibration.

Metrics were computed from out-of-fold predictions pooled across the ten folds. Accuracy was calculated as the proportion of correctly classified observations. Precision measured the proportion of predicted positive cases that were true positives, whereas recall measured the proportion of observed positive cases that the model correctly detected. The F1-score was calculated as the harmonic mean of precision and recall and was used to summarise the balance between omission and commission errors for the positive class. The area under the ROC curve (AUC) was used as a threshold-independent measure of class separability (Li, 2024), indicating the ability of the model to rank positive observations above negative observations. Precision, recall, and F1-score were considered particularly relevant because the vulnerability target was strongly imbalanced (D'Amico et al., 2021; Saito & Rehmsmeier, 2015).

To evaluate the potential influence of error propagation from the attack-transition maps to the risk model, an additional sensitivity analysis was performed. The original risk model, which included infestation-pressure variables derived from predicted attack-transition maps, was compared with two alternative formulations: (i) a no-pressure model excluding distance from previous attacks and local attack density, and (ii) a reference-pressure model in which these variables were replaced by distance and density metrics derived from photointerpreted infestation records for the corresponding observation year. All variants retained predicted vulnerability and static proximity variables and were evaluated using the same grouped cross-validation strategy.

In addition to cross-validation metrics, the spatial agreement between the original risk maps and the alternative risk maps was assessed using the Pearson correlation coefficient calculated on continuous probability values within the coastal pine-forest mask. Pearson's correlation coefficient was used as a descriptive measure of map similarity, following recent forest remote-sensing studies that used correlation-based comparisons to assess agreement among spatial products (Xiao et al., 2024). The coefficient measures the strength and direction of the linear association between two continuous variables and ranges from −1 to +1, with values close to +1 indicating strong positive agreement. In this analysis, the coefficient was computed pixel-wise for each annual risk map by comparing the original risk probability surface with the corresponding alternative probability surface. The resulting annual coefficients were then averaged across years. Because raster pixels are spatially autocorrelated and very numerous, Pearson correlation was used only as a descriptive measure of spatial similarity, and statistical significance tests were not interpreted.

Model interpretation

Model interpretation was based on model-based importance and SHAP values. Model-based importance was used to identify the most informative predictors within each component. SHAP values were computed for the vulnerability and risk models to assess the direction and magnitude of predictor effects and to support ecological interpretation of spectral, temporal, and spatial drivers.

To facilitate interpretation, SHAP values were analysed both at the individual-predictor level and after aggregation into predictor groups. Predictor groups distinguished Sentinel-2 bands, vegetation indices, absolute interannual differences, normalised interannual differences, infestation-pressure variables, and

spatial-proximity predictors. This aggregation was used to reduce overinterpretation of individual correlated spectral variables and to compare the relative contribution of different ecological and spatial information sources.

Area quantification and temporal consistency analysis

Annual probability maps were used to quantify the temporal evolution of infestation transition, vulnerability and risk across the 2017–2025 period. For each modelling product, two complementary area metrics were calculated. First, the probability-weighted area (i.e. the expected area obtained by weighting each pixel by its predicted probability) provides a threshold-independent estimate of the expected area affected, vulnerable, or at high risk. This metric was used to summarise model outputs without imposing an arbitrary probability threshold. Second, a high-probability area was calculated by applying model-specific thresholds to the probability maps.

Model-specific thresholds derived from cross-validation were used to identify high-probability areas. To evaluate the anticipatory consistency of vulnerability and risk products, high-vulnerability and high-risk areas predicted for year t were compared with high-probability attack areas mapped in year $t + 1$. For each year, were calculated the proportion of the future attack area falling within high-vulnerability and high-risk zones, along with an enrichment ratio. The enrichment ratio was defined as the proportion of future attacks captured by high-probability areas divided by the proportion of the total monitored pine forest area classified as high probability (Harris et al., 2024). Values greater than one indicate that high-vulnerability or high-risk areas captured future attacks more effectively than expected from their spatial extent alone. Together, these metrics linked the annual probability maps to both the temporal expansion of the infestation and the predictive value of vulnerability and risk maps.

Results

Model performance and spatial probability maps

The attack transition model showed moderate predictive performance under cross-validation, with a mean accuracy of 0.75 and an AUC of 0.79. The model achieved a precision of 0.61 and a recall of 0.52 for the transition class, indicating a reasonable compromise between false positives and missed attack events (Table 3). The vulnerability model showed high overall accuracy (0.88), but this was largely influenced by class imbalance. Its F1-score at the default classification setting was low, while the AUC reached 0.62 (Table 3). For this reason, vulnerability should be interpreted as a relative susceptibility area rather than as a reliable hard classification. The risk model outperformed vulnerability alone, with an accuracy of 0.90 and an AUC of 0.80 (Table 3). This suggests that infestation pressure and exposure variables provided information that was not captured by spectral susceptibility indicators alone. Fold-level cross-validation metrics are provided in Table S1.

The sensitivity analysis showed that the risk model remained stable when attack-derived pressure variables were removed or replaced by reference-based pressure metrics. The original risk model achieved a mean cross-validated AUC of 0.803, compared with 0.805 for the no-pressure formulation and 0.835 for the reference-pressure formulation. Spatial agreement with the original risk maps was also high, with mean Pearson correlations of 0.949 and 0.948 for the no-pressure and reference-pressure formulations, respectively. These results indicate that the risk product was not solely driven by error propagation from predicted attack-transition maps (Tables S2 and S3).

Table 3. Cross-validation performance of the Random Forest models for attack, vulnerability, and risk.

Model	Accuracy	Precision	Recall	F1-score	AUC
Attack transition	0.751	0.612	0.515	0.557	0.788
Vulnerability	0.879	0.100	0.008	0.015	0.621
Risk	0.899	0.797	0.235	0.345	0.802

The resulting maps provide three complementary spatial products: current attack transition, near-future vulnerability, and near-future risk. The three probability maps for the final observation year are shown in Figure 2.

Predictor importance and SHAP interpretation

The vulnerability model was mainly driven by red-edge, moisture-related, and temporal-change variables. The highest SHAP contribution was associated with REPO, followed by the normalised annual difference in NDMI. Sentinel-2 red-edge and visible bands, including B6, B5, and B2, also contributed substantially. Among temporal metrics, both absolute differences and normalised differences were important (Figure 3 and Table S4). At the group level, normalised differences accounted for 28.0% of the total SHAP contribution, followed by spectral indices (25.0%), Sentinel-2 bands (23.5%), and absolute differences (23.4%) (Figure S2 and Table S5). The normalised-difference group was only slightly more influential than the absolute-difference group, suggesting that both the absolute magnitude and the relative intensity of spectral change contributed to vulnerability prediction.

The risk model was dominated by predicted vulnerability and infestation-pressure variables. Predicted vulnerability had the largest SHAP value, followed by distance from previously attacked areas and attack density. Spatial proximity predictors, including proximity to coast, roads, and railways, provided additional but smaller contributions (Figure 3 and Table S4). At the group level, infestation pressure and vulnerability accounted for approximately three-quarters of the total SHAP contribution (75.5%), whereas spatial proximity accounted for the remaining quarter (24.5%) (Figure S2 and Table S5). This indicates that risk was primarily shaped by the interaction between susceptible canopy conditions and spatial exposure to previous infestation patterns.

Annual attack, vulnerability and risk areas

The monitored pine-forest area was consistently close to 4,357 ha across years. The probability-weighted attack area ranged from approximately 1,499 ha in 2018 to 1,777 ha in 2023, corresponding to 34.4–40.8% of the monitored pine forests. The extent of high-probability attack areas increased from 1,144 ha in 2018 to a maximum of 1,570 ha in 2023. A clear increase was observed in 2023, followed by a partial reduction in 2024 and 2025 (Figure 4, while the full annual values are reported in Table S4).

The probability-weighted vulnerability area ranged from approximately 668 ha to 992 ha, with the highest value in the 2025 observation year for the 2026 target year (Table 4 and Figure 4, while the full annual values are reported in Table S6). The F1-optimised vulnerability threshold was low (0.09), reflecting the strong imbalance of the near-future attack target and the use of vulnerability as a screening product. Consequently, the corresponding high-vulnerability area covered a large proportion of the monitored pine forests and should not be interpreted as a high-severity class. Risk maps were more spatially selective, with probability-weighted risk area ranging from 775 to 1,231 ha, and high-risk area from 734 to 1,360 ha. The highest risk extent occurred in the 2025 observation year for the 2026 target year.

Anticipatory consistency of vulnerability and risk maps

High-vulnerability areas captured a large proportion of next-year predicted attacks, ranging from 74.8% to 86.5%. However, because the selected vulnerability threshold classified a large fraction of the study area as high vulnerability, enrichment ratios were modest, ranging from 1.17 to 1.30 (Figure 5; full annual overlap statistics are reported in Table S7). In contrast, high-risk areas captured a smaller proportion of next-year attacks, ranging from 32.2% to 44.6%, but did so over a much smaller portion of the landscape. Consequently, risk maps showed stronger enrichment, with ratios ranging from 1.64 to 2.00 (Figure 5; full annual overlap statistics are reported in Table S7). This indicates that the risk model provided a more spatially selective early-warning area than vulnerability alone (Table 5).

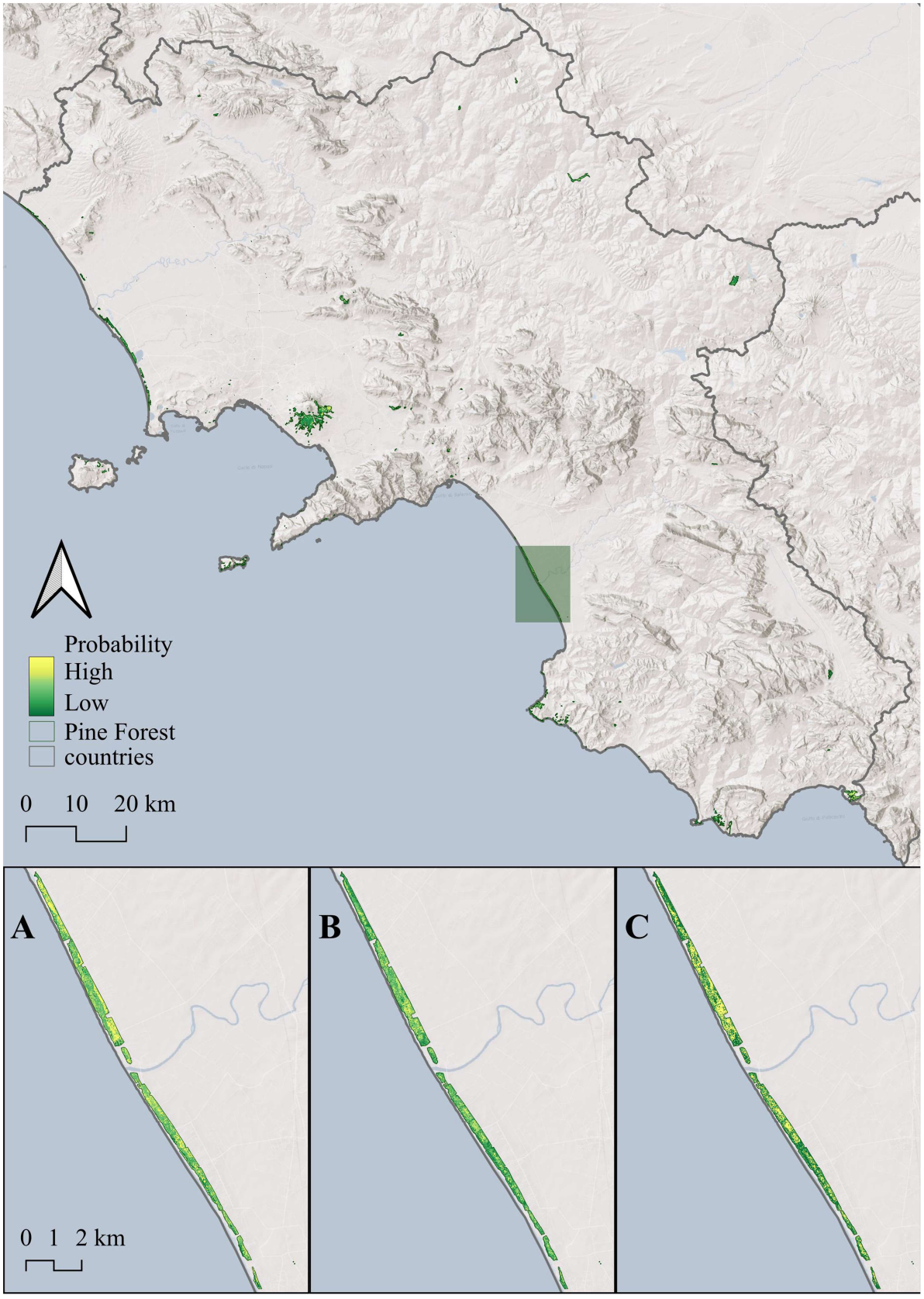

Figure 2. Spatial probability maps for the final observation year showing (A) attack transition for 2025, (B) vulnerability, and (C) risk for the 2026 target year.

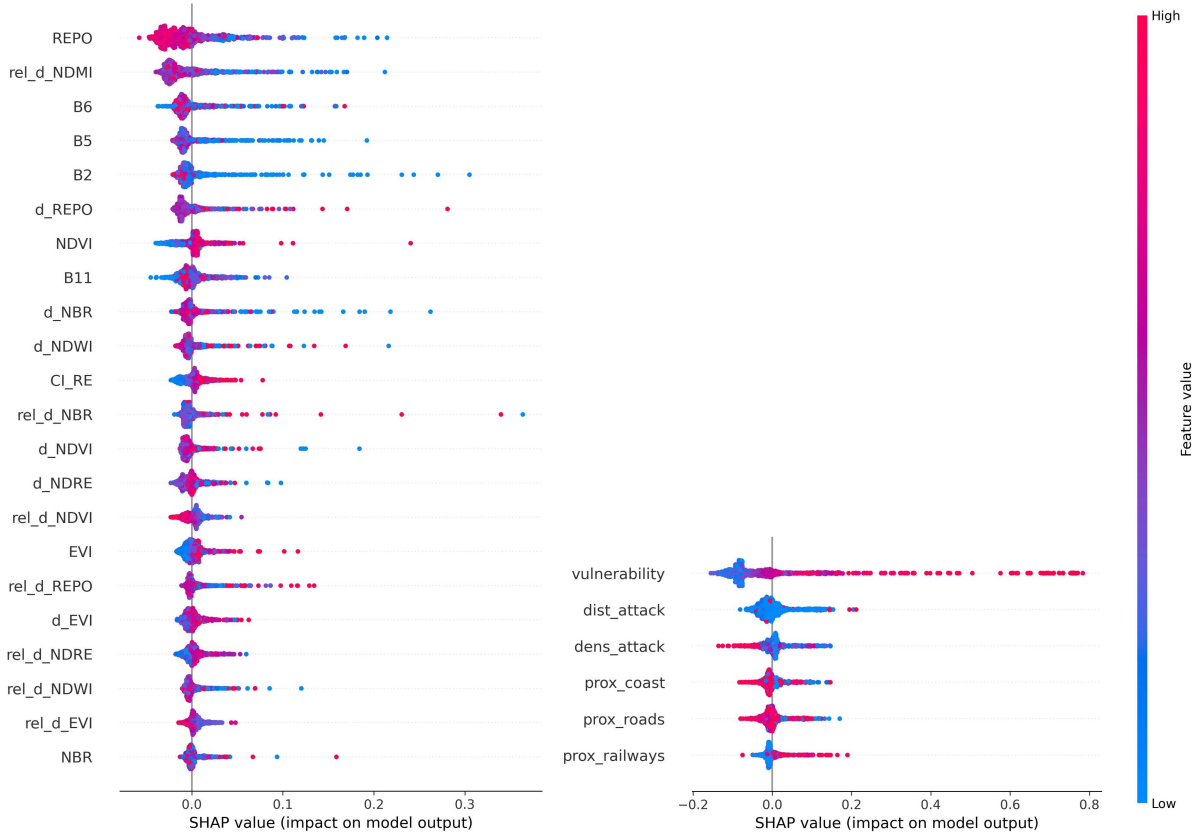

Figure 3. Individual predictor variable contribution to vulnerability (left) and risk (right) according to the SHAP interpretation of the respective models. Positive SHAP values increase the predicted probability of the target class. Predictor values are shown from low to high, allowing interpretation of both predictor importance and direction of effect.

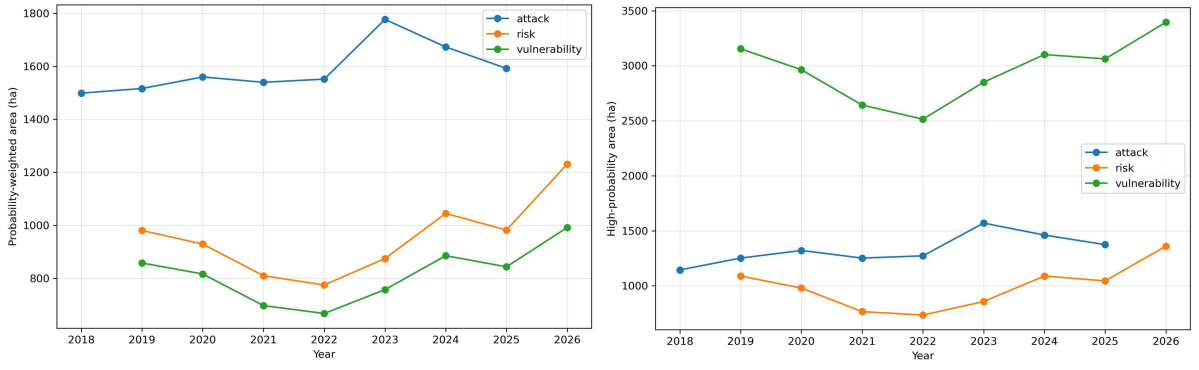

Figure 4. Temporal evolution of probability-weighted area and high-probability area for attack transition, vulnerability, and risk across the monitored coastal pine forests.

Discussion

Reference data consistency

The temporal consistency check showed that several Sentinel-2 predictors associated with canopy greenness, moisture status, and red-edge response displayed coherent changes around the assigned onset year (Figure S1). In particular, NDVI, NDMI, NBR, EVI, NDRE, and CI_RE generally showed lower mean values around or after the assigned onset than in the preceding years. This supports the plausibility of the

Table 4. Summary of annual area statistics for attack, vulnerability and risk products.

Product	Threshold	Mean monitored area (ha)	Min probability-weighted area (ha)	Max probability-weighted area (ha)	Mean probability-weighted area (%)	Min high area (ha)	Max high area (ha)	Mean high area (%)
Attack	0.500	4356.3	1498.8	1776.6	36.46	1144.1	1569.9	30.55
Vulner.	0.090	4356.3	667.8	991.9	18.71	2514.3	3395.2	67.96
Risk	0.280	4356.3	775.2	1231.3	21.89	734.0	1360.2	22.72

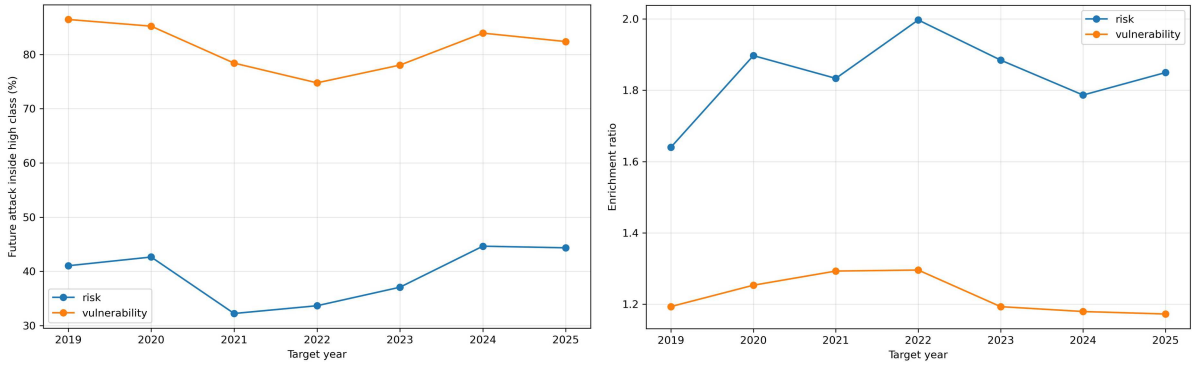

Figure 5. Anticipatory consistency of vulnerability and risk maps, showing the percentage of next-year high-probability attack area captured by high-vulnerability and high-risk areas, and corresponding enrichment ratio. Values greater than one indicate that high-probability areas captured future attack more effectively than expected from their spatial extent alone.

Table 5. Anticipatory consistency of high vulnerability and high risk areas with next-year attack maps.

Predictor map	Mean future attack captured (%)	Min captured (%)	Max captured (%)	Mean enrichment ratio	Min enrichment	Max enrichment	Mean high-area share (%)
Vulnerability	81.32	74.77	86.46	1.23	1.17	1.30	66.53
Risk	39.37	32.22	44.64	1.84	1.64	2.00	21.51

photointerpreted temporal attribution, while also highlighting that infestation onset should be interpreted with an expected uncertainty of approximately ±1 year.

Sentinel-2 indicators of Toumeyella-related canopy decline

Sentinel-2 summer observations captured canopy responses associated with *T. parvicornis* decline, although the contribution of individual predictors differed among modelling objectives. In the attack-transition model, the most important variables were mainly spectral indices and interannual differences, including NBR, CI_RE, REPO, and normalised differences in NDMI, NBR and NDWI. This indicates that infestation onset was associated with canopy degradation, chlorophyll-related responses and moisture-sensitive spectral changes. These findings are consistent with previous studies on *T. parvicornis*, which showed that vegetation indices and Sentinel-2 time series can capture canopy decline in affected *Pinus pinea* stands (Nicoletti et al., 2024; Niccoli et al., 2024; Petti et al., 2026).

For vulnerability, SHAP values highlighted the importance of red-edge position, normalised NDMI change and red-edge bands. The prominence of REPO and B5–B6 suggests that vulnerability was linked to subtle shifts in the red-edge region, consistent with changes in chlorophyll content and canopy physiological status, in agreement with previous Sentinel-2 studies characterising forest canopy properties (D'Amico et al., 2024; Immitzer et al., 2019). The relevance of red-edge and moisture-sensitive predictors is also consistent with the physiological interpretation of pest-induced decline, in which chlorophyll reduction, canopy thinning and water-related stress alter NIR, red-edge and SWIR responses (Bascietto et al., 2025).

However, because Sentinel-2 bands, vegetation indices and interannual differences are partly correlated and often describe related physiological or structural canopy properties, the individual SHAP ranking should not be interpreted as a strict hierarchy of independent ecological drivers. A more robust interpretation is that the vulnerability model relied on a coherent spectral-temporal predictor cluster

combining red-edge and chlorophyll-related information, moisture-sensitive responses and annual change metrics. In this sense, predictors such as REPO, normalised NDMI change and red-edge bands should be interpreted as representative of broader red-edge, moisture and temporal-change signals rather than as isolated causal variables.

This interpretation is supported by the group-level SHAP results (Figure S2 and Table S5). Normalised differences, spectral indices, Sentinel-2 bands and absolute differences showed similar contributions, indicating that vulnerability information was distributed across multiple correlated Sentinel-2 predictor groups. Both absolute and normalised interannual differences were informative, suggesting that early susceptibility was associated not only with the magnitude of spectral decline but also with the relative change from the previous-year condition. This is particularly relevant in heterogeneous pine stands, where identical absolute declines may correspond to different levels of canopy stress depending on the initial physiological condition (Senf et al., 2017), and is consistent with studies showing that temporal trajectories often provide more disturbance-related information than single-date observations (Candotti et al., 2022; Lastovicka et al., 2020).

Spatial drivers of infestation risk

The risk model improved discrimination over vulnerability alone, as shown by the increase in AUC from 0.62 to 0.80. This supports the conceptual separation adopted in the study: vulnerability describes spectral predisposition to future decline, whereas risk emerges when susceptibility is combined with exposure to infestation sources and potential dispersal pathways. The SHAP results confirmed that vulnerability alone was insufficient to explain near-future attack probability. Predicted vulnerability, distance from previous attacks and local attack density formed the dominant vulnerability/infestation-pressure cluster, indicating that the regional spread of *T. parvicornis* was not only associated with local canopy conditions but also with spatial contagion and neighbourhood pressure.

Transportation-related and coastal proximity variables contributed less than the vulnerability/infestation-pressure cluster, but they were retained in the risk model and provided additional explanatory information. These variables should not be interpreted as direct causal drivers but rather as spatial exposure proxies related to transport corridors, coastal gradients, and local landscape configuration. This interpretation is consistent with dispersal-oriented studies showing a decreasing probability of infestation with increasing distance from initial hotspots, and with recent evidence suggesting that wind alone may not fully explain local spread patterns of *T. parvicornis* (Bascietto et al., 2025; Candotti et al., 2026; Garonna et al., 2018). Therefore, as for the vulnerability model, the risk interpretation should focus primarily on predictor clusters rather than on the exact ranking of individual distance or proximity variables. The main ecological distinction is between the vulnerability/infestation-pressure cluster and the spatial-proximity cluster (Figure S2 and Table S5).

Implications for monitoring and management

The framework provides three complementary maps for forest-health monitoring. Attack maps reconstruct the spatial progression of likely infestation onset; vulnerability maps identify stands with a spectral predisposition to near-future decline; risk maps integrate susceptibility and exposure and are therefore better suited to prioritising surveillance. The overlap analysis showed that risk maps were more spatially selective than vulnerability maps, capturing roughly one third to nearly half of next-year attack within about one fifth of the landscape and with enrichment ratios close to two. This is consistent with recent multi-platform monitoring studies emphasising the operational value of combining Sentinel-2 with higher-resolution imagery and field/photo-interpretation data for timely surveillance of pine decline (Falanga et al., 2024; Nicoletti et al., 2024; Petti et al., 2026).

Limitations

Several limitations should be considered. First, the reference dataset was derived from occurrence observations revised through photointerpretation, and the exact onset of infestation remains uncertain

where symptoms developed gradually. Second, Sentinel-2 pixels integrate canopy and background signals over 10 m, which may be limiting in narrow or fragmented coastal pine stands.

Third, the vulnerability and risk products should be interpreted according to their different levels of robustness. The vulnerability model showed modest cross-validated discrimination and should therefore be interpreted primarily as a relative susceptibility surface or high-sensitivity screening layer, rather than as a binary diagnostic product. The thresholded vulnerability map is best understood as an operational screening layer, whereas continuous probability maps and probability-weighted area estimates provide a more robust representation of vulnerability patterns. Unlike the infestation-pressure variables used in the risk model, the vulnerability layer did not directly inherit errors from predicted attack-transition maps, because it was estimated from Sentinel-2 predictors using next-year infestation occurrence as the target. Nevertheless, its uncertainty may still propagate into the risk product, which combines predicted vulnerability with spatial exposure variables. Fourth, although grouped cross-validation avoided assigning observations from the same reference point to both training and validation folds, it does not completely remove residual spatial dependence among neighbouring observations. This may have led to optimistic performance estimates, particularly for the risk model, which explicitly includes infestation-pressure variables. However, these variables were intentionally included to represent local spatial contagion and exposure within the operational monitoring area, rather than to support extrapolation to independent regions. In this context, grouped cross-validation was considered the most appropriate validation strategy because it reduced temporal leakage among repeated observations while preserving class balance and infestation-year representation in a geographically narrow and discontinuous coastal study area. Future applications should test the framework using independent regions or spatially structured validation designs when larger and more spatially balanced reference datasets become available. Fifth, thresholds derived from F1 optimisation were useful for comparison but may not align with management severity classes. Therefore, thresholded maps should be interpreted as operational prioritisation layers rather than as severity classes, while continuous probability maps and probability-weighted area estimates provide a more robust representation of spatial patterns. Sixth, although the proposed framework is conceptually transferable to other Mediterranean coastal pine forests, external validation in additional regions is still required before broad operational application can be recommended. Finally, variable importance measures in tree-based models may be affected by correlation among predictors, especially when spectral bands and derived indices are used together (Strobl et al., 2008). Therefore, SHAP values should be interpreted as indicators of model contribution rather than causal importance, particularly in the presence of correlated Sentinel-2 bands and vegetation indices. Consequently, ecological interpretation should primarily rely on predictor groups rather than on the exact ranking of individual variables (Lundberg & Lee, 2017; Molnar, 2022) (Figure S2).

Conclusions

This study developed an interpretable Sentinel-2 framework to reconstruct infestation dynamics, vulnerability, and risk associated with *T. parvicornis* in Mediterranean coastal pine forests of Campania. The analysis showed that summer Sentinel-2 indicators, particularly red-edge, moisture-sensitive, and inter-annual change metrics, were informative for detecting canopy decline and susceptibility patterns. Vulnerability was associated with REPO, normalised NDMI change and red-edge/visible bands, while risk was mainly controlled by predicted vulnerability and spatial pressure from previous attacks.

The results highlight the importance of distinguishing between infestation detection, forest vulnerability, and spatial risk. The vulnerability layer provides a high-sensitivity screening product that identifies broad patterns of forest susceptibility, although it should not be interpreted as a stand-alone predictive model. In contrast, integrating vulnerability with infestation pressure and spatial exposure variables produced more selective risk maps with stronger enrichment for next-year attacks, making the risk model the most suitable product for early-warning surveillance and operational prioritisation. The proposed workflow is therefore suitable for regional monitoring and early-warning applications in Mediterranean pine forests affected by invasive pests, while also providing interpretable evidence of the spectral and spatial drivers associated with the spread of infestation.

Acknowledgements

This study was partially supported via the following projects: 1. FORWARDS "The ForestWard Observatory to Secure Resilience of European Forests", HORIZON project funded by the European Commission, number 101084481 call HORIZON-CL6-2022-CLIMATE-01. 2. MONIFUN. H2020 project funded by the European Commission, number 101134991 call HORIZON-CL6-2023-CircBio-01-14. 3. NextGenCarbon. H2020 project funded by the European Commission, number 101184989 call HORIZON-CL5-2024-D1-01-07.

Author contributions

CRediT: **Giovanni D'Amico:** Conceptualization, Methodology, Supervision, Writing – original draft, Writing – review & editing.

Disclosure statement

No potential conflict of interest was reported by the author(s).

During manuscript preparation, ChatGPT (OpenAI, GPT-5.5 Pro) was used to support language editing, restructuring, and clarity of selected sections. The author reviewed and edited all AI-assisted text and takes full responsibility for the scientific content, analyses, interpretations, references, and conclusions. No AI tool was used to generate research data, model outputs, or research figures.

Data availability statement

Sentinel-2 Level-2A Surface Reflectance Harmonised data are freely available through the Google Earth Engine platform (COPERNICUS/S2_SR_HARMONIZED). The original *Toumeyella parvicornis* occurrence data are publicly available from the Campania Regional Plant Protection Service (https://agricoltura.regione.campania.it/difesa/toumeyella.html). Road and railway infrastructure data are available from the Regione Campania open data portal (https://dati.regione.campania.it/catalogo/datasetdetail/rete-viaria). Coastline data are available from the ISPRA SINACLOUD coastal database (https://sinacloud.isprambiente.it/portal/apps/sites/#/coste/pages/dati). The forest mask used in this study was derived from the Italian Forest Map available through the SINFOR platform (https://cfi-sinfor.crea.gov.it/Home/CartaForestale). The revised reference dataset, processing scripts, model outputs and derived maps generated in this study are available from the corresponding author upon reasonable request.

References

Andresini, G., Appice, A., & Malerba, D. (2023). SILVA: An eXplainable framework to map bark beetle infestation in Sentinel-2 images. *IEEE Journal of Selected Topics in Applied Earth Observations and Remote Sensing*, *16*, 10050–10066. https://doi.org/10.1109/JSTARS.2023.3312521

Bonari, G., Fernández-González, F., Çoban, S., Monteiro-Henriques, T., Bergmeier, E., Didukh, Y. P., Chytrý, M., Xystrakis, F., Angiolini, C., Acosta, A. T., Agrillo, E., Costa, J. C., Danihelka, J., Hennekens, S. M., Kavgacı, A., Knollová, I., Neto, C. S., Sağlam, C., Škvorc, Ž., … Ewald, J. (2021). Classification of the Mediterranean lowland to submontane pine forest vegetation. *Applied Vegetation Science*, *24*(1), e12544. https://doi.org/10.1111/avsc.12544

Bárta, V., Lukeš, P., & Homolová, L. (2021). Early detection of bark beetle infestation in Norway spruce forests of central Europe using Sentinel-2. *International Journal of Applied Earth Observation and Geoinformation*, *100*, 102335. https://doi.org/10.1016/j.jag.2021.102335

Bascietto, M., Chirici, G., Mastrogregori, E., Oreti, L., Palma, A., Tiberini, A., & Bertin, S. (2025). Detecting symptoms and dispersal of pine tortoise scale pest in an urban forest by remote sensing. *Land*, *14*(3), 630. https://doi.org/10.3390/land14030630

Belgiu, M., & Drăguţ, L. (2016). Random forest in remote sensing: A review of applications and future directions. *ISPRS journal of photogrammetry and remote sensing*, *114*, 24–31. https://doi.org/10.1016/j.isprsjprs.2016.01.011

Bonari, G., Acosta, A. T., & Angiolini, C. (2017). Mediterranean coastal pine forest stands: Understorey distinctiveness or not? *Forest ecology and management*, *391*, 19–28. https://doi.org/10.1016/j.foreco.2017.02.002

Bozzini, A., Francini, S., Chirici, G., Battisti, A., & Faccoli, M. (2023). Spruce bark beetle outbreak prediction through automatic classification of Sentinel-2 imagery. *Forests*, *14*(6), 1116. https://doi.org/10.3390/f14061116

Breiman, L. (2001). Random forests. *Machine learning*, *45*(1), 5–32. https://doi.org/10.1023/A:1010933404324

Candotti, A., De Giglio, M., Dubbini, M., & Tomelleri, E. (2022). A Sentinel-2 based multi-temporal monitoring framework for wind and bark beetle detection and damage mapping. *Remote Sensing*, *14*(23), 6105. https://doi.org/10.3390/rs14236105

Candotti, A., Fassnacht, F. E., Malenovský, Z., & Tomelleri, E. (2026). Recent advances in remote sensing for early detection, risk prediction, and post-disturbance assessment of bark beetle attacks in temperate and boreal forests. *Current Forestry Reports*, *12*(1), 11. https://doi.org/10.1007/s40725-026-00272-0

D'Amico, G., Nilsson, M., Axelsson, A., & Chirici, G. (2024). Data homogeneity impact in tree species classification based on Sentinel-2 multitemporal data case study in central Sweden. *International Journal of Remote Sensing*, *45*(15), 5050–5075. https://doi.org/10.1080/01431161.2024.2371082

D'Amico, G., Francini, S., Parisi, F., Vangi, E., De Santis, E., Travaglini, D., & Chirici, G. (2023). Multitemporal optical remote sensing to support forest health condition assessment of Mediterranean pine forests in Italy. In *Global Challenges for a Sustainable Society* (pp. 113–123). Springer. https://doi.org/10.1007/978-3-031-25840-4_15

D'Amico, G., Francini, S., Giannetti, F., Vangi, E., Travaglini, D., Chianucci, F., Chirici, G., Mattioli, W., Grotti, M., Puletti, N., & Corona, P. (2021). A deep learning approach for automatic mapping of poplar plantations using Sentinel-2 imagery. *GIScience & Remote Sensing*, *58*(8), 1352–1368. https://doi.org/10.1080/15481603.2021.1988427

Dalponte, M., Solano-Correa, Y. T., Frizzera, L., & Gianelle, D. (2022). Mapping a european spruce bark beetle outbreak using Sentinel-2 remote sensing data. *Remote sensing*, *14*(13), 3135. https://doi.org/10.3390/rs14133135

Delegido, J., Verrelst, J., Alonso, L., & Moreno, J. (2011). Evaluation of sentinel-2 red-edge bands for empirical estimation of Green LAI and chlorophyll content. *Sensors*, *11*(7), 7063–7081. https://doi.org/10.3390/s110707063

Di Sora, N., Contarini, M., Rossini, L., Turco, S., Brugneti, F., Metaliaj, R., Speranza, S., Vejsiu, I., & Peri, L. (2024). First report of toumeyella parvicornis (Cockerell)(Hemiptera: Coccidae) in Albania and its potential spread in the coastal area of the balkans. *EPPO Bulletin*, *54*(2), 160–165. https://doi.org/10.1111/epp.13014

Drusch, M., Del Bello, U., Carlier, S., Colin, O., Fernandez, V., Gascon, F., Bargellini, P., Hoersch, B., Isola, C., Laberinti, P., Martimort, P., Meygret, A., Spoto, F., Sy, O., & Marchese, F. (2012). Sentinel-2: ESA's optical high-resolution mission for GMES operational services. *Remote sensing of Environment*, *120*, 25–36. https://doi.org/10.1016/j.rse.2011.11.026

EFSA Panel on Plant Health (PLH). Bragard, C., Baptista, P., Chatzivassiliou, E., Di Serio, F., Gonthier, P., & MacLeod, A. (2022). Pest categorisation of toumeyella parvicornis. *EFSA Journal*, *20*(3), e07146. https://doi.org/10.2903/j.efsa.2022.7146

EPPO. (2026). *Toumeyella parvicornis*. *EPPO Global Database*. Online May: https://gd.eppo.int/taxon/TOUMPA/distribution/IT

Falanga, V., Francini, S., Parisi, F., Cavalli, A., De Fioravante, P., Cucca, B., Marchetti, M., D'Amico, G., Chirici, G., Lasserre, B., Ottaviano, M., & Munafò, M. (2024). Near-real-time detection of insect outbreaks in urban trees using a PlanetScope time series. *Forests*, *15*(12), 2261. https://doi.org/10.3390/f15122261

Flood, N. (2013). Seasonal composite landsat TM/ETM+ images using the medoid (a multi-dimensional median). *Remote Sensing*, *5*(12), 6481–6500. https://doi.org/10.3390/rs5126481

Forzieri, G., Girardello, M., Ceccherini, G., Mauri, A., Spinoni, J., Beck, P., Feyen, L., & Cescatti, A. (2020). *Vulnerability of European forests to natural disturbances* (pp. 1831–9424). Luxembourg: Publications Office of the European Union. ISBN 978-92-76-13884-6. https://doi.org/10.2760/736558

Gao, B. C. (1996). NDWI—A normalized difference water index for remote sensing of vegetation liquid water from space. *Remote sensing of environment*, *58*(3), 257–266. https://doi.org/10.1016/S0034-4257(96)00067-3

Garonna, A. P., Scarpato, S., Vicinanza, F., & Espinosa, B. (2015). First report of toumeyella parvicornis (Cockerell) in Europe (Hemiptera: Coccidae). *Zootaxa*, *3949*(1), 142–146. https://doi.org/10.11646/zootaxa.3949.1.9

Garonna, A. P., Foscari, A., Russo, E., Jesu, G., Somma, S., Cascone, P., & Guerrieri, E. (2018). The spread of the non-native pine tortoise scale toumeyella parvicornis (Hemiptera: Coccidae) in Europe: A major threat to pinus pinea in Southern Italy. *IForest*, *11*(5), 628–634. https://doi.org/10.3832/ifor2864-011

Gholizadeh, A., Mišurec, J., Kopačková, V., Mielke, C., & Rogass, C. (2016). Assessment of red-edge position extraction techniques: A case study for Norway spruce forests using hymap and simulated sentinel-2 data. *Forests*, *7*(10), 226. https://doi.org/10.3390/f7100226

Gitelson, A. A., Gritz, Y., & Merzlyak, M. N. (2003). Relationships between leaf chlorophyll content and spectral reflectance and algorithms for non-destructive chlorophyll assessment in higher plant leaves. *Journal of plant physiology*, *160*(3), 271–282. https://doi.org/10.1078/0176-1617-00887

Goodwin, N. R., Coops, N. C., Wulder, M. A., Gillanders, S., Schroeder, T. A., & Nelson, T. (2008). Estimation of insect infestation dynamics using a temporal sequence of landsat data. *Remote sensing of environment*, *112*(9), 3680–3689. https://doi.org/10.1016/j.rse.2008.05.005

Gorelick, N., Hancher, M., Dixon, M., Ilyushchenko, S., Thau, D., & Moore, R. (2017). Google earth engine: Planetary-scale geospatial analysis for everyone. *Remote sensing of Environment*, *202*, 18–27. https://doi.org/10.1016/j.rse.2017.06.031

Harris, J., Pirtle, J. L., Laman, E. A., Siple, M. C., & Thorson, J. T. (2024). An ensemble approach to species distribution modelling reconciles systematic differences in estimates of habitat utilization and range area. *Journal of Applied Ecology*, *61*(2), 351–364. https://doi.org/10.1111/1365-2664.14559

Hlásny, T., Zimová, S., Merganičová, K., Štěpánek, P., Modlinger, R., & Turčáni, M. (2021). Devastating outbreak of bark beetles in the Czech Republic: Drivers, impacts, and management implications. *Forest Ecology and Management*, *490*, 119075. https://doi.org/10.1016/j.foreco.2021.119075

Huete, A., Didan, K., Miura, T., Rodriguez, E. P., Gao, X., & Ferreira, L. G. (2002). Overview of the radiometric and biophysical performance of the MODIS vegetation indices. *Remote sensing of environment*, *83*(1-2), 195–213. https://doi.org/10.1016/S0034-4257(02)00096-2

Huo, L., Koivumäki, N., Oliveira, R. A., Hakala, T., Markelin, L., Näsi, R., Honkavaara, E., Suomalainen, J., Polvivaara, A., & Junttila, S. (2024). Bark beetle pre-emergence detection using multi-temporal hyperspectral drone images: Green shoulder indices can indicate subtle tree vitality decline. *ISPRS Journal of Photogrammetry and Remote Sensing*, *216*, 200–216. https://doi.org/10.1016/j.isprsjprs.2024.07.027

Immitzer, M., Neuwirth, M., Böck, S., Brenner, H., Vuolo, F., & Atzberger, C. (2019). Optimal input features for tree species classification in central Europe based on multi-temporal Sentinel-2 data. *Remote Sensing*, *11*(22), 2599. https://doi.org/10.3390/rs11222599

IPCC. (2012). Managing the risks of extreme events and disasters to advance climate change adaptation, (p. 582). The Edinburgh Building, Shaftesbury Road, Cambridge CB2 8RU ENGLAND: Cambridge University Press Available from June 2012.

Key, C. H., & Benson, N. C. (2006). Landscape assessment (LA), *Lutes, Duncan C.; Keane, Robert E.; Caratti, John F.; Key, Carl H.; Benson, Nathan C.; Sutherland, Steve; Gangi, Larry J. 2006. FIREMON: Fire effects monitoring and inventory system. Gen. Tech. Rep. RMRS-GTR-164-CD* (p. LA-1-55, 164). Fort Collins, CO: US Department of Agriculture, Forest Service, Rocky Mountain Research Station.

Lastovicka, J., Svec, P., Paluba, D., Kobliuk, N., Svoboda, J., Hladky, R., & Stych, P. (2020). Sentinel-2 data in an evaluation of the impact of the disturbances on forest vegetation. *Remote Sensing*, *12*(12), 1914. https://doi.org/10.3390/rs12121914

Li, J. (2024). Area under the ROC curve has the most consistent evaluation for binary classification. *PLoS One*, *19*(12), e0316019. https://doi.org/10.1371/journal.pone.0316019

Lundberg, S. M., & Lee, S. I. (2017). A unified approach to interpreting model predictions. *Advances in neural information processing systems*, *30*. https://doi.org/10.48550/arXiv.1705.07874

McFeeters, S. K. (1996). The use of the normalized difference water index (NDWI) in the delineation of open water features. *International journal of remote sensing*, *17*(7), 1425–1432. https://doi.org/10.1080/01431169608948714

Molnar, C. (2022). Interpretable Machine Learning: A Guide for Making Black Box Models Explainable. ISBN 9798411463330.

Niccoli, Francesco, Kabala, Jerzy Piotr, Altieri, Simona, Faugno, Salvatore, & Battipaglia, Giovanna. (2024). Impact of Toumeyella parvicornis outbreak in Pinus pinea L. forest of Southern Italy: First detection using a dendro-chronological, isotopic and remote sensing analysis. *Forest Ecology and Management*, 566, 122086. https://doi.org/10.1016/j.foreco.2024.122086

Nicoletti, R., De Masi, L., Migliozzi, A., & Calandrelli, M. M. (2024). Analysis of dieback in a coastal pinewood in campania, Southern Italy, through high-resolution remote sensing. *Plants*, *13*(2), 182. https://doi.org/10.3390/plants13020182

Park Williams, A., Allen, C. D., Macalady, A. K., Griffin, D., Woodhouse, C. A., Meko, D. M., McDowell, N. G., Swetnam, T. W., Rauscher, S. A., Seager, R., Grissino-Mayer, H. D., Dean, J. S., Cook, E. R., Gangodagamage, C., & Cai, M. (2013). Temperature as a potent driver of regional forest drought stress and tree mortality. *Nature climate change*, *3*(3), 292–297. https://doi.org/10.3389/fpls.2013.00266

Petti, B., D'Amico, G., Alvites, C., Parisi, F., Bambagioni, E., Bruno, R., Francini, S., Santopuoli, G., Lassere, B., Chirici, G., Ottaviano, M., & Marchetti, M. (2026). Remote sensing across scales and platforms: Monitoring castelporziano nature reserve forest insect outbreaks. *Rendiconti Lincei. Scienze Fisiche e Naturali*, *37*, 1–13. https://doi.org/10.1007/s12210-025-01387-5

Regione Campania. (2025). *Monitoraggio Toumeyella parvicornis in Campania.* Regional Plant Protection Service. https://agricoltura.regione.campania.it/comunicati/comunicato_11-03-25.html

Rouse, J. W., Jr, Haas, R. H., Schell, J. A., & Deering, D. W. (1973). Monitoring the vernal advancement and retrogradation (green wave effect) of natural vegetation (No. NASA-CR-132982).

Sommerfeld, A., Senf, C., Buma, B., D'Amato, A. W., Després, T., Díaz-Hormazábal, I., Seidl, R., Fraver, S., Frelich, L. E., Gutiérrez, ÁG., Hart, S. J., Harvey, B. J., He, H. S., Hlásny, T., Holz, A., Kitzberger, T., Kulakowski, D., Lindenmayer, D., Mori, A. S., … Veblen, T. T. (2018). Patterns and drivers of recent disturbances across the temperate forest biome. *Nature communications*, *9*(1), 4355. https://doi.org/10.1038/s41467-018-06788-9

Saito, T., & Rehmsmeier, M. (2015). The precision-recall plot is more informative than the ROC plot when evaluating binary classifiers on imbalanced datasets. *PLoS One*, *10*(3), e0118432. https://doi.org/10.1371/journal.pone.0118432

Seidl, R., Thom, D., Kautz, M., Martin-Benito, D., Peltoniemi, M., Vacchiano, G., Reyer, C. P., Wild, J., Ascoli, D., Petr, M., Honkaniemi, J., Lexer, M. J., Trotsiuk, V., Mairota, P., Svoboda, M., Fabrika, M., & Nagel, T. A. (2017). Forest disturbances under climate change. *Nature climate change*, *7*(6), 395–402. https://doi.org/10.1038/nclimate3303

Senf, C., & Seidl, R. (2021). Persistent impacts of the 2018 drought on forest disturbance regimes in Europe. *Biogeosciences*, *18*(18), 5223–5230. https://doi.org/10.5194/bg-18-5223-2021

Senf, C., Seidl, R., & Hostert, P. (2017). Remote sensing of forest insect disturbances: Current state and future directions. *International journal of applied earth observation and geoinformation*, *60*, 49–60. https://doi.org/10.1016/j.jag.2017.04.004

Stone, C., & Mohammed, C. (2017). Application of remote sensing technologies for assessing planted forests damaged by insect pests and fungal pathogens: A review. *Current Forestry Reports*, *3*(2), 75–92. https://doi.org/10.1007/s40725-017-0056-1

Strobl, C., Boulesteix, A. L., Kneib, T., Augustin, T., & Zeileis, A. (2008). Conditional variable importance for random forests. *BMC Bioinformatics*, *9*(1), 307. https://doi.org/10.1186/1471-2105-9-307

Tagarelli, N., Avosani, S., Tucci, M., & Verrastro, V. (2022). First report of toumeyella parvicornis (Hemiptera: Coccidae) in puglia (south-eastern Italy). *EPPO Bulletin*, *52*(2), 487–492. https://doi.org/10.1111/epp.12849

Xiao, Y., Wang, Q., & Zhang, H. K. (2024). Global natural and planted forests mapping at fine spatial resolution of 30 m. *Journal of Remote Sensing*, *4*, 0204. https://doi.org/10.34133/remotesensing.0204